

# Electron density fluctuations in a Hall plasma thruster: observations by collective light scattering

Sedina TSIKATA<sup>1)</sup>, Nicolas LEMOINE<sup>2)</sup>, Vitaliy PISAREV<sup>1)</sup> and Dominique GRESILLON<sup>1)</sup>

<sup>1)</sup>Laboratoire de Physique et Technologie des Plasmas, CNRS, Ecole Polytechnique, Palaiseau, France

<sup>2)</sup>Laboratoire de Physique des Milieux Ionisés et Applications, CNRS, Université Henri-Poincaré, Nancy, France

(Received: 1 September 2008 / Accepted: 10 November 2008)

A new collective light scattering diagnostic was built to investigate electron density fluctuations and associated instabilities in a Hall thruster plasma. Previous numerical simulations have predicted electronic transport across magnetic field lines occurring at the scales of the electron cyclotron drift radius at certain frequencies. This paper presents the first experimental observations of the electron density fluctuations in the expected ranges of wave number and frequency, supporting the role of these instabilities in anomalous electronic diffusion. Key features such as the dispersion relations, form factor and spatial distribution of these fluctuations are discussed.

Keywords: light scattering, Hall thruster, electron density fluctuations, instabilities, form factor

## 1. Introduction

The improvement of Hall plasma thrusters poses challenges because the physics underlying their operation has not yet been fully mastered. A key question concerns the origin of the large electron temperature and anomalous electronic transport across magnetic field lines in the thruster. In the past, this phenomenon was explained via wall collisions [1], however, the electron-wall collision frequency was shown to be too small to account for the unexpectedly large electron mobility and temperature.

Yoshikawa and Rose [2] showed early on that density fluctuations could give rise to anomalous diffusion. Hybrid codes and two-dimensional particle-in-cell simulations [3] have since given ample support for the notion that turbulence accounts for the anomalous heating and transport. In particular, oscillations perpendicular to the magnetic field, of frequencies on the order of a few MHz, and of characteristic length scales close to 1mm, were predicted to have an influence on transport. Reliable experimental measurements of the electron density fluctuations inside the thruster plasma have been, however, hard to come by.

Previous experimental work on the thruster has focused on the use of antennae or probes on the edge of the plasma to identify large-scale oscillations in the thruster [4]. Our thruster investigations use, for the first time, a non-invasive collective light scattering diagnostic (PRAXIS) to study electron density fluctuations in the thruster plume at small scales. This study presents several new experimental results on electron density fluctuations.

## 2. Experimental details

The thruster is operated (typically at a Xenon flow rate of 20mg/s) in a cylindrical vacuum vessel

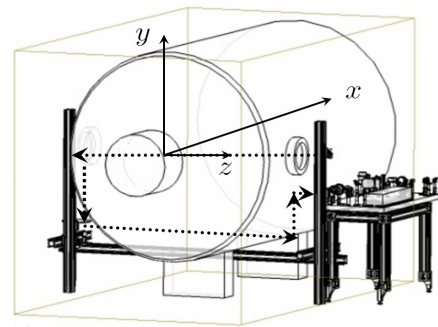


Fig. 1 Setup of the collective scattering diagnostic, with the PRAXIS optical bench beside the vacuum vessel. The dotted lines show the path followed by the laser beams, which intersect in front of the thruster exit plane and are returned to a detector on the bench. The x-axis corresponds to the thruster axis.

(radius 1.1m) and is situated on the vessel axis near the front of the vessel, with an axial displacement of the thruster possible. A beam from a continuous power, 10.6 $\mu$ m wavelength, 42W laser on the PRAXIS optical bench is split into two beams, consisting of a low-power, frequency-shifted local oscillator and an intense primary beam, which cross in the thruster plume. This defines both the scattering volume and the scattering wave vector  $\mathbf{k}$ . The thruster plume is accessible via a ZnSe window on one side of the vessel. The primary and local oscillator beams and the scattered radiation are collected through a diametrically opposite window on the vessel. The local oscillator beam and the scattered radiation are sent to a detector on the bench (Fig. 1).

The waist of the beams in the scattering region is 2.5mm. Scattering angles of 6 to 20mrad were investigated, and in the current study, the wave vector was

author's e-mail: sedina.tsikata@polytechnique.edu

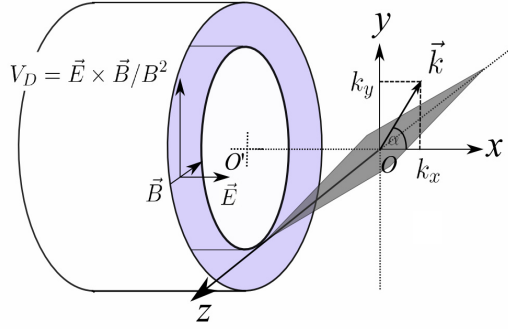


Fig. 2 View of the front of the thruster. The axes shown correspond to those of Fig. 1, with the x axis aligned with the thruster axis. The radial B-field and axial E-field are indicated, as is the direction of the  $\mathbf{E} \times \mathbf{B}$  electron drift. The dark grey lozenge corresponds to the observation volume, while the light gray annulus corresponds to a plasma region (which forms the thruster plume at the exterior of the thruster). The observation vector  $\mathbf{k}$  forms an angle  $\alpha$  with the x-axis.

oriented parallel to the  $\mathbf{E} \times \mathbf{B}$  drift direction or parallel to the thruster axis. Fig. 2 provides details of the coordinate system, the orientations of the thruster electric and magnetic fields, and the wave vector orientation.

In Fig. 2,  $\alpha$  is the angle between  $\mathbf{k}$  and the horizontal ion beam, and the results in this study correspond to two angles,  $0^\circ$  ( $\mathbf{k}$  oriented parallel to the ion beam) and  $90^\circ$  ( $\mathbf{k}$  oriented parallel to the  $\mathbf{E} \times \mathbf{B}$  drift). The scattering volume is at least 20cm in length, traversing the thruster diameter.

## 2.1 Signal processing

Heterodyne detection is used to generate a complex signal which is proportional to the spatial Fourier transform of the electron density, at a particular scattering wave vector  $\mathbf{k}$ .

The signal from the detector is amplified and demodulated into its real and imaginary parts by the second, analogous stage of the heterodyne detection. A record of typical length  $6.5 \times 10^6$  samples, at a rate of 50MHz, is made simultaneously on the two channels and stored on a computer. Four types of records are made: (i) the laser signal without the plasma, (ii) the signal with the detector closed, (iii) the signal with the plasma and laser beams present, and (iv) the signal with only the primary beam absent. These records are used to determine the true scattered signal and the true photonic noise and subsequently, the intensity of the scattered signal.

## 2.2 Form factor normalization

The large depth of memory allows for an improvement of the signal to noise ratio via an averaging procedure. A Fourier analysis is performed on a short slice of samples (eg. 200). All the resulting  $N$  spectra ( $N$  = total length of records/slice length) are then averaged. This yields a mean Fourier frequency spectrum with a variance reduced by  $\sqrt{N}$  (eg. about 180).

The scattered signal spectral density,  $I(k, \omega)$ , is normalized by the photonic noise spectral density,  $I_{ph}(k, \omega)$ , to yield the dynamic form factor  $S(k, \omega)$ , in units of seconds (Eq. 1):

$$S(k, \omega) = \frac{h\nu\pi\omega^2}{\eta P_o \lambda^2 r_o^2 n_o L} \frac{I(k, \omega)}{I_{ph}(k, \omega)} \quad (1)$$

In Eq. 1,  $\frac{h\nu}{\eta P_o}$  is the ratio of the photon energy to the efficient laser power,  $n_o$  is a mean plasma density (assumed to be  $10^{18} m^{-3}$ ), and  $L$  is the length of the observation lozenge.

This normalization eliminates variations in amplifier gain in the electronics circuit and removes other signal artefacts. The static form factor (later used in Fig. 6) is the dynamic form factor integrated over an appropriate frequency range and provides an absolute measure of the fluctuation intensity at a given wave vector.

## 3. General observations

The diagnostic and data treatment permitted the observation of clear signals at low (below 1MHz) and high (1-25MHz) frequencies. Only the general observations at high frequencies are presented here.

### 3.1 Characteristic frequency spectra

Fig. 3 and Fig. 4 show two normalized frequency spectra obtained for a wave vector oriented parallel to the  $\mathbf{E} \times \mathbf{B}$  drift and parallel to the ion beam, respectively.

In Fig. 3,  $\mathbf{k}$  is parallel to  $\mathbf{E} \times \mathbf{B}$ . The wave number is 5900 rad/m and the observation lozenge is situated 13.5mm from the thruster exit plane. This spectrum is characterized by an intense frequency peak near 2.5MHz (and a smaller symmetric negative peak).

In Fig. 4,  $\mathbf{k}$  is parallel to the ion beam. The wave number is 6500 rad/m and the observation lozenge is situated 12.5mm from the thruster exit plane. The spectrum peak is much less intense and is situated near 20MHz.

The very sharp peak at 0 MHz in Fig. 3 is due to stray diffraction and does not constitute the principal signal of the diffusion. Features of the very low frequency peaks, such as are evident in Fig. 4, will not be discussed here.

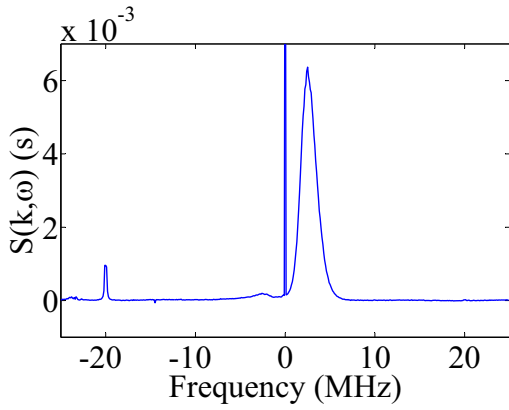


Fig. 3 A characteristic normalized frequency spectrum obtained with  $\mathbf{k}$  oriented parallel to the  $\mathbf{E} \times \mathbf{B}$  drift. The principal signal is around 2.5MHz.

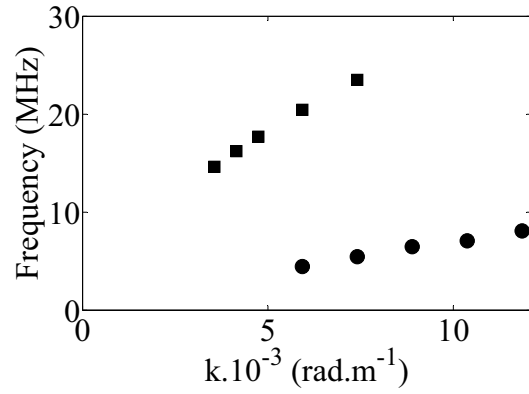


Fig. 5 Characteristic dispersion relations for different  $\mathbf{k}$  orientations.  $\mathbf{k}$  parallel to the  $\mathbf{E} \times \mathbf{B}$  drift (circles), and  $\mathbf{k}$  parallel to the ion beam direction (squares). The observation volume is 7.5mm from the motor exit plane.

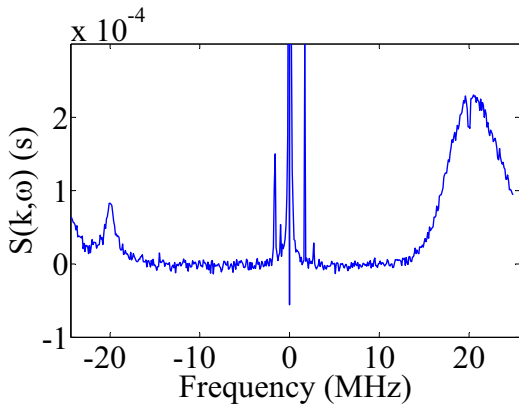


Fig. 4 A characteristic normalized frequency spectrum obtained with  $\mathbf{k}$  oriented parallel to the ion beam direction. The principal signal is around 20MHz.

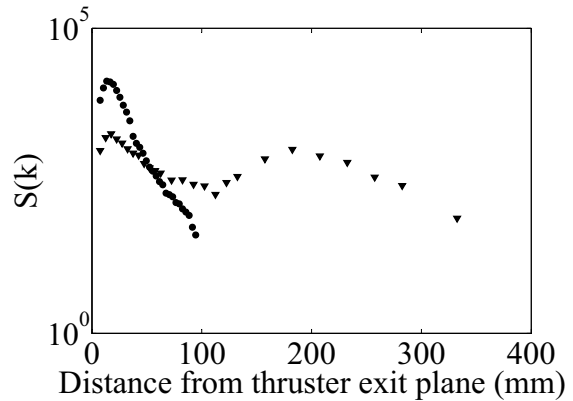


Fig. 6 The static form factor magnitude  $S(k)$  as a function of distance from the thruster exit plane for  $\mathbf{k}$  parallel to the  $\mathbf{E} \times \mathbf{B}$  drift (circles) and  $\mathbf{k}$  parallel to the ion beam direction (triangles). The wavenumber in both cases is 6200 rad/m.

### 3.2 Dispersion relations

The variation of frequency with wave number was examined for  $\mathbf{k}$  parallel to the  $\mathbf{E} \times \mathbf{B}$  drift and to the ion beam. In both orientations, a linear variation of the frequency with wave vector was observed, however, characteristic velocities in the two directions were quite different. An example of two characteristic dispersion relations is shown in Fig. 5.

In Fig. 5, electron density fluctuations along  $\mathbf{E} \times \mathbf{B}$  are characterized by a group velocity of 4300 m/s. Variation of the Xe input flow rate has no effect on the linear shape and slope of the dispersion relation.

Fluctuations along the ion beam are characterized by a group velocity of around 16000 m/s. This value is very close to the ion beam velocity in the exhaust plume.

### 3.3 Spatial distribution of density fluctuations

The fluctuation intensity was studied as a function of axial distance from the thruster. Results of this study for the two different  $\mathbf{k}$  orientations are shown in Fig. 6.

For both orientations of  $\mathbf{k}$ , the largest density fluctuations occur not right at the thruster exit plane, but about 13.5mm from it. For  $\mathbf{k}$  parallel to  $\mathbf{E} \times \mathbf{B}$ , the form factor shows an exponential drop after the maximum value and the fluctuations disappear 100mm from the thruster exit plane. In contrast, density fluctuations along the ion beam direction persist over the entire distance which was accessible during this experiment.

### 3.4 Our results in the context of theoretical models

Adam *et al.* [3] showed that the electron drift velocity was a source of an instability which could heat the electrons and cause transport across magnetic field lines. Our diagnostic is capable of examining this instability (with  $\mathbf{k}$  oriented along  $\mathbf{E} \times \mathbf{B}$ ) and strong density fluctuations are seen in this direction. Significantly, the diagnostic validated the presence of this instability at the frequency range and wavelengths predicted in numerical codes. In comparison, previous experimental studies indicated the presence of instabilities at scales two orders of magnitude larger than in the current study. Our work is the first experimental study of electron density fluctuations at the millimeter scale.

The numerical results predicted the existence of unstable modes only for certain discrete values of wavenumber. Let us define  $\rho_{CD}$  as the Larmor radius of an electron moving at the  $\mathbf{E} \times \mathbf{B}$  drift velocity. According to theory, unstable modes occur for integer values of  $k\rho_{CD}$  larger than 1. For our experiment,  $1.5 < k\rho_{CD} < 3.3$ ; the unstable modes predicted should be evident at  $k\rho_{CD} = 2, 3$ . However, even when the resolution of the diagnostic is taken into account, the theoretical results do not concur with the continuous dispersion relation in this regime, which is what is observed experimentally.

This study provides several new measurements of electron density fluctuations in a Hall thruster. Important similarities and differences with the results of numerical codes are already apparent; work is ongoing to develop coherent theoretical models for the observations and to understand the implications of this work on existing models for anomalous transport.

- [1] A.I. Morozov and V.V. Savelyev, *Rev. Plasma Fluids* **21**, 277 (2000).
- [2] S. Yoshikawa and D.J. Rose, *Phys. Fluids* **5**, 334 (1962).
- [3] J.C. Adam, A. Héron and G. Laval, *Phys. Plasmas* **11**, 295 (2004).
- [4] A. Lazurenko, V. Vial, M. Prioul and A. Bouchoule, *Phys. Plasmas* **12**, 013501 (2005).